International Journal of Pharmaceutics 635 (2023) 122753

Contents lists available at ScienceDirect

International Journal of Pharmaceutics

journal homepage: www.elsevier.com/locate/ijpharm

Lipid-based nanoparticles: Enhanced cellular uptake via surface thiolation

Patrick Knoll [a], Giuseppe Francesco Racaniello [b], Valentino Laquintana [b], Florina Veider [a], Ahmad Saleh [a,c], Anna Seybold [d], Nunzio Denora [b], Andreas Bernkop-Schnürch [a,*]

[a] Center for Chemistry and Biomedicine, Department of Pharmaceutical Technology, Institute of Pharmacy, Leopold-Franzens-University of Innsbruck, Innrain 80/82, 6020 Innsbruck, Austria
[b] Department of Pharmacy – Pharmaceutical Sciences, University of Bari "Aldo Moro", Italy
[c] Department of Pharmacy, Universitas Mandala Waluya, A.H.Nasution, Kendari 93231, Southeast Sulawesi, Republic of Indonesia
[d] Department of Zoology, University of Innsbruck, 6020 Innsbruck, Austria

ARTICLE INFO

Keywords:
Nanostructured lipid carriers
Thiolation
Cellular uptake
Endocytosis
Uptake mechanism
Permeation

ABSTRACT

The aim of this study was to evaluate the uptake mechanism of thiolated nanostructured lipid carriers (NLCs). NLCs were decorated with a short-chain polyoxyethylene(10)stearyl ether with a terminal thiol group (NLCs-PEG_{10}-SH) or without (NLCs-PEG_{10}-OH) as well as with a long-chain polyoxyethylene(100)stearyl ether with thiolation (NLCs-PEG_{100}-SH) or without (NLCs-PEG_{100}-OH). NLCs were evaluated for size, polydispersity index (PDI), surface morphology, zeta potential and storage stability over six months. Cytotoxicity, adhesion to the cell surface and internalization of these NLCs in increasing concentrations were evaluated on Caco-2 cells. The influence of NLCs on the paracellular permeability of lucifer yellow was determined. Furthermore, cellular uptake was examined with and without various endocytosis inhibitors as well as reducing and oxidizing agents. NLCs were obtained in a size ranging from 164 to 190 nm, a PDI of 0.2, a negative zeta potential < -33 mV and stability over six months. Cytotoxicity was shown to be concentration dependent and to be lower for NLCs with shorter PEG chains. Permeation of lucifer yellow was 2-fold increased by NLCs-PEG_{10}-SH. All NLCs displayed concentration dependent adhesion to the cell surface and internalization, which was in particular 9.5-fold higher for NLCs-PEG_{10}-SH compared to NLCs-PEG_{10}-OH. Short PEG chain NLCs and especially thiolated short PEG chain NLCs showed higher cellular uptake than NLCs with longer PEG chain. Cellular uptake of all NLCs was mainly clathrin-mediated endocytosis. Thiolated NLCs showed also caveolae-dependent and clathrin- and caveolae-independent uptake. Macropinocytosis was involved in NLCs with long PEG chains. NLCs-PEG_{10}-SH indicated thiol-dependent uptake, which was influenced by reducing and oxidizing agents. Due to thiol groups on the surface of NLCs their cellular uptake and paracellular permeation enhancing properties can be substantially improved.

1. Introduction

Lipid-based nanocarriers have recently attracted worldwide attention as several vaccines against the coronavirus disease are based on such formulations. However, these nanocarriers still struggle with obstacles such as poor cellular uptake when administered orally (Kali et al., 2022). A new approach to improve the cellular uptake is the use of thiolated polymers called thiomers, which were developed in the late 1990s (Leichner et al., 2019). Thiolated polymers are capable of forming disulfide bonds between endogenous cysteines and thiol groups being covalently attached to polymers (Irmukhametova et al., 2011). This interaction enables several beneficial functions of thiomers such as high mucoadhesion, inhibition of enzymes, efflux pump inhibition and permeation enhancing effects (Bonengel and Bernkop-Schnürch, 2014;

Abbreviations: NLCs, nanostructured lipid carriers; PEG, polyoxyethylene glycol; PDI, polydispersity index; NLCs-PEG_{10}-OH, polyoxyethylene(10)stearyl ether; NLCs-PEG_{100}-OH, polyoxyethylene(100)stearyl ether; NLCs-PEG_{10}-SH, thiolated polyoxyethylene(10)stearyl ether; NLCs-PEG_{100}-SH, thiolated polyoxyethylene(100) stearyl ether; CH_2Cl_2, dichloromethane; NBS, N-bromosuccinimide; PPh_3, triphenylphosphine; Ph_3PO, triphenylphosphine oxide; DMF, N,N-dimethylformamide; LGR, lumogen red; EFTEM, energy-filtered transmission electron microscopy; SQV, saquinavir; MEM, minimum essential medium; FBS, fetal bovine serum; HBS, HEPES buffered saline; LDH, lactate dehydrogenase; TEER, transepithelial electrical resistance; LY, lucifer yellow; MβCD, methyl-β-cyclodextrin; GSH, glutathione; H_2O_2, hydrogen peroxide.

* Corresponding author.
E-mail address: Andreas.Bernkop@uibk.ac.at (A. Bernkop-Schnürch).

https://doi.org/10.1016/j.ijpharm.2023.122753
Received 20 December 2022; Received in revised form 9 February 2023; Accepted 15 February 2023
Available online 1 March 2023

Grassiri et al., 2022; Russo et al., 2016). In recent years, researchers have focused on transferring the advantageous properties of thiolated polymers to lipid-based nanocarriers (Bhat et al., 2021; Wibel et al., 2021). Since poor drug solubility and low bioavailability after oral administration of highly lipophilic drugs are still major obstacles in drug delivery, lipid-based nanocarriers such as nanostructured lipid carriers (NLCs) were developed to address these shortcomings (Beloqui et al., 2016). Up to date, however, poor cellular uptake of NLCs remains a challenge (Gómez-Guillén and Montero, 2021; Kali et al., 2022). A promising strategy seems to be the design of thiolated nanocarriers, which have shown enhanced cellular uptake (Jiang et al., 2013; Meng et al., 2014). Nanocarriers have been thiolated in the past using various methods such as coating nanocarriers with thiolated polymers (Wibel et al., 2021). Such coatings, however, are not always stable and can be removed by the harsh intestinal environment (Friedl et al., 2021). A more stable alternative might be the thiolation of the hydrophilic head group of surfactants whose lipophilic tails are firmly anchored in the lipid phase of nanocarriers. In a previous study, NLCs decorated with a thiolated PEGylated surfactant showed increased mucus interactions with porcine intestinal mucosa (Racaniello et al., 2022). For successful drug delivery, however, also their cellular uptake properties have to be high. Safwat et al. have already pointed out the great potential of PEGylated NLCs, which exhibit high cellular uptake (Safwat et al., 2017). A promising strategy to further improve the uptake might be the decoration of lipid-based drug delivery systems with thiolated surfactants. Some of the best known viruses such as HIV, coronaviruses and hepatitis virus are internalized via a thiol-mediated mechanism (Laurent et al., 2021). The concept of a thiol-mediated internalization has so far been applied to only a few types of lipid-based formulations (Hock et al., 2022; Torres and Gait, 2012). In particular, the uptake mechanism of thiolated NLCs has not yet been fully explored. In general, nanocarriers are internalized via different endocytosis pathways by intestinal epithelial cells after oral administration (Rennick et al., 2021). Since different pathways affect the efficacy of drug uptake significantly, the development of nanocarriers that are to a high extent endocytosed may improve the bioavailability of incorporated drugs. For instance, nanocarriers, that are internalized by caveolae-dependent endocytosis, have a higher chance to escape lysosomal degradation (Li et al., 2015). A shift from clathrin-mediated endocytosis to more caveolae-mediated endocytosis through surface modification of NLCs may improve the uptake efficiency of nanocarriers. In addition, understanding the signaling pathways can help to predict the performance of nanocarriers when transferred from in vitro to in vivo (Rennick et al., 2021). To predict the oral efficiency of a drug delivery system, Caco-2 cells are the most common tool for simulating the epithelium (Artursson et al., 2012).

The aim of this study was therefore to evaluate the cellular uptake of thiolated NLCs and to provide details on the underlying mechanism. A short-chain polyoxyethylene(10)stearyl ether (NLCs-PEG_{10}-OH), and its thiolated version (NLCs-PEG_{10}-SH) were used for the decoration of NLCs. To investigate the influence of the PEG chain length, NLCs were additionally decorated with a long-chain polyoxyethylene(100)stearyl ether (NLCs-PEG_{100}-OH) and its thiolated modification (NLCs-PEG_{100}-SH). NLCs were evaluated for their size, polydispersity index (PDI), surface morphology, zeta potential, and long-term storage stability. Cytotoxicity as well as adhesion to the cell surface and internalization were investigated in increasing concentrations on Caco-2 cells. In addition, the effect of thiolated NLCs on the permeation of lucifer yellow across a Caco-2 cell monolayer was evaluated. To analyze the underlying uptake mechanism of thiolated NLCs, cellular uptake was determined at 4 °C and in the presence of various endocytosis inhibitors. Furthermore, the influence of a reducing and an oxidizing agent on thiol-dependent uptake was studied.

2. Materials and methods

2.1. Materials

Cetyl palmitate (>98%) was obtained from Thermo Fisher Scientific (Massachusetts, USA). Oleic acid, penicillin, streptomycin, phosphate buffered saline (PBS), trypsin and fetal bovine serum (FBS) were purchased from Merck KGaA (Darmstadt, Germany). Acetone was received by DonauChem (Vienna, Austria). Pluronic F68 and Lumogen F Red 300 were a kind gift from BASF (Ludwigshafen, Germany). N-bromosuccinimide (NBS), triphenylphosphine, thiourea, dichloromethane, polyoxyethylene (10) stearyl ether, polyoxyethylene (100) stearyl ether, minimum essential medium eagle (MEM), resazurin sodium salt, potassium chloride, calcium chloride, sodium chloride (≥99.5%), bovine serum albumin, Triton-X 100, trypan blue (0.4%), chlorpromazine (≥98%), methyl- β-cyclodextrin, quercetin (≥95%), hydrogen peroxide 30% (w/w) in H_2O, L-glutathione reduced and lucifer yellow dipotassium salt were obtained by Sigma-Aldrich (Vienna, Austria). 4-(2-Hydroxyethyl)-1-piperazineethanesulfonic acid (HEPES, ≥99.5%) and nystatin dihydrate (≥4,400 I.U./mg) were purchased from Roth GmbH (Karlsruhe, Germany). D-Glucose anhydrous (≥99.5%) and rottlerin were received from VWR Chemicals (Solon, USA).

2.2. Thiolation of surfactants

Thiolated polyoxyethylene (10) stearyl ether (S10 SH) and polyoxyethylene (100) stearyl ether (S100 SH) were synthesized as previously described (Racaniello et al., 2022). In brief, polyoxyethylene (10) stearyl ether (S10 OH) and polyoxyethylene (100) stearyl ether (S100 OH) were each added in a final concentration of 1.0 mmol to a 5 mL of dichloromethane (CH_2Cl_2) solution of 1.1 mmol N-bromosuccinimide (NBS) and 1.0 mmol triphenylphosphine (PPh_3) to substitute the terminal hydroxyl groups by bromine. The mixture was stirred overnight at 40 °C. The solution was then cooled to room temperature. Triphenylphosphine oxide (Ph_3PO) was precipitated by adding diethyl ether in the same volume. After storage overnight at 0 °C, the precipitate was eliminated by centrifugation (SL 16R Centrifuge, Thermo Scientific, USA) at 13000 rpm at 4 °C for 15 min. The solvent was evaporated by a rotavapor (BUCHI Italia Srl). After dissolving the brominated intermediate in 2 mL of N,N-dimethylformamide (DMF), a solution of 25 mg of thiourea in 5 mL of DMF was added. The mixture was stirred overnight at 90 °C using a condenser. The thiolated products were dried using a rotavapor and purified by column chromatography. As a stationary phase served a silica gel 60 with 230–240 mesh and as mobile phase an acetone/ CH_2Cl_2 mixture of equal volumes was used. The purified products were dried by a rotavapor and stored at 4 °C until further use. To quantify the thiols of the modified surfactants, Ellman's test and disulfide test were performed as described previously (Knoll et al., 2021). A comprehensive structural characterization of thiolated surfactants was performed previously (Racaniello et al., 2022).

2.3. Preparation of NLCs

NLCs were prepared as previously described with minor modifications (Racaniello et al., 2022). 80 mg of cetyl palmitate, 20 mg of oleic acid and 12 mg of unthiolated and thiolated polyoxyethylene (10) stearyl ether (S10 OH and S10 SH), polyoxyethylene (100) stearyl ether (S100 OH and S100 SH) were dissolved in 500 μL of acetone. As aqueous phase, 5 mL of a 1% (*m/v*) Pluronic F68 solution was prepared. The lipid phase was heated up to 50 °C at 500 rpm using a thermomixer (ThermoMixer C, Eppendorf Vertrieb Deutschland GmbH, Germany). The water phase was warmed up to the same temperature. The clear lipid

solution was then added to the aqueous phase and stirred for 25 min in order to evaporate the acetone. To further homogenize NLCs, the particle dispersion was sonicated for 2.5 min using a sonicator at 100% amplitude and 0.75 Hz. Afterwards, NLCs were formed and cooled down on ice. Water that evaporated during ultrasonication was replenished. After cooling NLCs on ice, the nanocarriers were stored in a refrigerator until further use. The concentration of NLCs was expressed as the weight of lipids per volume of aqueous phase throughout this manuscript. For quantification, NLCs were additionally loaded with lumogen red (LGR) by dissolving 0.5% (*m/v*) LGR in the lipid phase of NLCs before preparing the NLCs as described above.

2.4. Evaluation of size, polydispersity index (PDI), zeta potential and storage stability

NLCs were characterized regarding size, polydispersity index and zeta potential using Zetasizer Nano ZS (Malvern Instruments, UK). Therefore, nanocarriers were diluted 1:20 with demineralized water and incubated for 10 min at 37 °C at 300 rpm. The size and PDI were measured via photon correlation spectroscopy with a backscatter angle of 173° using a He-Ne laser at a wavelength of 633 nm. Zeta potential was determined by electrophoretic light scattering at a scattering angle of 12.8° utilizing a dip cell (Malvern Instruments, UK). The measurements were carried out at 37 °C in triplicate. Stability studies were performed under continuous shaking at 300 rpm at 37 °C for 24 h. To determine long-term stability, NLCs were stored at 4 °C for 6 months and analyzed for size and PDI.

2.5. Characterization of morphology

Surface and shape morphology of NLCs were evaluated by energy-filtered transmission electron microscopy (EFTEM) (Wibel et al., 2021). NLCs were diluted with demineralized water 1:10 and transferred on 200 mesh Formvar/carbon-coated copper grids (Balzers Union, Liechtenstein). After drying, NLCs were analyzed by a Zeiss Libra 120 (Carl Zeiss AG, Oberkochen, Germany). EFTEM images were taken by a 2 × 2 k high-speed camera (Troendle, Germany) and ImageSP software (Troendle, Germany).

2.6. Preparation and evaluation of saquinavir loaded NLCs

NLCs are particularly designed for the delivery of highly lipophilic drugs of low bioavailability (Muchow et al., 2008). Therefore, the BCS IV drug saquinavir (SQV) was loaded into the lipid phase of NLCs that were characterized regarding size, PDI, zeta potential, drug load and encapsulation efficiency. Briefly, SQV was dissolved in the lipid phase in a concentration of 3% (*m/v*). The subsequent preparation was performed as described above for the unloaded NLCs. The drug load and encapsulation efficiency were determined as previously described (Knoll et al., 2022). 500 μL of SQV loaded NLCs were transferred to Amicon centrifugal filters (Merck, Tutzing, Germany) with a molecular weight cut-off of 100 kDa. After centrifugation at 2000 rpm and 4 °C for 20 min, unencapsulated SQV was quantified in the filtrate by HPLC by injection of 50 μL of sample. Analytics were performed using an Elite LaChrom HPLC composed by a KNAUER Eurospher 100–5 reverse phase C18 column with precolumn (250 × 4 mm, 5 μm) as the stationary phase, an L-2200 autosampler, a L-2130 pump, and an L-2450 diode array detector (VWR Hitachi, Vienna, Austria). As mobile phase served 0.1% TFA (*v/v*) and acetonitrile (60/40). The SQV peak was detected at a wavelength of 354 nm and an elution time of 3.5 min for a total analysis run time of 10 min. SQV was quantified by generating a calibration curve ranging from 0.001 to 100 μg/mL ($R^2 > 0.99$).

Drug load was calculated as follows:

$$\text{Drug loading}\ (\mu g/mg) = \frac{total\ drug\ amount - unencapsulated\ drug\ amount}{total\ lipid\ content}$$

The encapsulation efficiency was calculated by the following equation:

$$\text{Encapsulation efficiency}\ (\%) = \frac{total\ drug\ amount - unencapsulated\ drug\ amount}{total\ drug\ amount}$$

2.7. Cell studies

Cell studies were performed with Caco-2 cells. Cells were seeded in an experiment dependent concentration in 24 and 96 well plates as described below. During the growth period, cells were stored in minimum essential medium (MEM) at 37 °C, 95% relative humidity, and 5% CO_2. MEM consisted of 10% (*v/v*) heat-inactivated fetal bovine serum (FBS) and penicillin/streptomycin solution (100 units/0.1 mg/L). Every two days, the MEM was replaced until the day of the experiment.

2.7.1. Cytotoxicity

NLCs were evaluated regarding their cytotoxicity in several concentrations as described previously (Jalil et al., 2020). Caco-2 cells were seeded in 96-well plates in 100 μL MEM in a density of 5×10^4 cells per well. The experiment was conducted when cells reached confluency. NLCs were prepared in sterile HEPES buffered saline (HBS) composed by 20 mM HEPES, 1 g/L glucose anhydrous, 136.7 mM NaCl, 5 mM KCl and 1 mM $CaCl_2$ in the concentrations of 0.01%, 0.05%, 0.10%, 0.50%, 1.00% and 2.00% (*m/v*). HBS alone, which is not harmful to cells, was used as a negative control. A 0.1% (*v/v*) Triton-X 100 solution in HBS was administered on cells as positive control. Before addition of NLCs, cells were washed three times with prewarmed HBS. After 4 h incubation, cells were washed again three times. Subsequently, HBS was replaced with a 0.1% (*m/v*) resazurin solution in HBS and incubated for 2 h. Cell viability was determined photometrically at an excitation wavelength of 540 nm and an emission wavelength of 590 nm. For this purpose, 100 μL of each well were transferred into a black 96-well plate to measure the fluorescence intensity. Cell viability was determined by the following equation:

$$\text{Cell viability}\ (\%) = \frac{intensity\ of\ sample - intensity\ of\ negative\ control}{intensity\ of\ positive\ control - intensity\ of\ negative\ control} \text{x}\ 100$$

To investigate whether NLCs cause membrane damage leading to cell death, an additional toxicity study was performed by determination of lactate dehydrogenase (LDH) release from cells that exhibited membrane leakage. Caco-2 cells were cultured and treated the same way as described above. After 12 h incubation of NLCs on cells, LDH was detected following the assay instructions of the provider (Promega, CytoTox-ONE™ Homogeneous Membrane Integrity Assay). LDH release was quantified photometrically at an excitation wavelength of 560 nm and an emission wavelength of 590 nm. Cytotoxicity was calculated as LDH release in percentage of LDH release in the presence of a 0.1% (*v/v*) Triton-X 100 solution.

2.7.2. Permeation across Caco-2 cell monolayer

NLCs were evaluated regarding their influence on the permeation across a Caco-2 cell monolayer. Caco-2 cells were seeded in a density of 2.5×10^4 cells per well on inserts of a 24-transwell plate with 1.13 cm^2 permeation area. The experiment was conducted after 21 days of cultivation. Two days before the experiment the media of donor and acceptor chamber was replenished by MEM without phenol red. The transepithelial electrical resistance (TEER) of each cell layer was determined before each study. Only wells showing a TEER value over 800 Ωcm^2 were considered for the experiment. NLCs were prepared in a concentration of 0.05% (*m/v*). To determine the influence of the thiolated and unthiolated NLCs on the permeation, lucifer yellow (LY) was added to the samples in a final concentration of 0.1% (*m/v*) as a marker for paracellular permeation. Then, 100 µL of each sample were transferred to the donor chambers. A 0.1% (*m/v*) LY solution in MEM was incubated on cells and served as control. The permeation study was conducted at 37 °C for three hours in an incubator. Every 30 min 100 µL were transferred from the acceptor chamber to a black microtiter plate. The withdrawn volume was replenished by fresh prewarmed medium. The fluorescence intensity of permeated LY was determined photometrically at an excitation wavelength of 434 nm and an emission wavelength of 540 nm. Results were evaluated as percentage of permeated LY. The apparent permeability coefficient (P_{app}) for LY was calculated as described in the following equation:

$$P_{app} = \frac{Q}{A \times c \times t}$$

where Q stands for the total amount LY permeated within 3 h, A is the diffusion area, c equates to the concentration of LY incubated on cells inside the donor chamber and t is the total time of the permeation study. The enhancement ratio was calculated by the quotient of P_{app} of sample through P_{app} of LY alone.

2.7.3. Adhesion to the cell surface and internalization of NLCs

To investigate the extent to which NLCs are superficially attached and fully internalized, cells were treated with 0.5% (m/v) LGR-labeled NLCs at various concentrations. Caco-2 cells were seeded on 24 well plates in 500 µL MEM at a cell density of 2.5×10^4 cells per well. The experiment was conducted after confluence and differentiation of cells was attained. The cells were first washed three times with HBS to remove MEM. NLCs were prepared in HBS in the concentrations 0.01%, 0.025%, 0.05%, and 0.075% (*m/v*) and incubated on cells for three hours at 37 °C. Thereafter, nanocarriers were washed off by adding and removing of ice-cold phosphate buffered saline (PBS) for three times. At the last time, PBS was kept on cells and 150 µL of 4% (*v/v*) Triton-X 100 was added to each well to lyse cells. After 30 min incubating at 37 °C in an orbital shaker (Incubator ES-80, Grant Instruments Ltd., Cambridge, England) at 200 rpm, 100 µL of each well were transferred to a black microtiter plate. The fluorescence intensity was determined photometrically at 575/610 nm excitation and emission wavelength, respectively. A calibration curve was generated by treating the cells simultaneously without washing off the NLCs after incubation. Cell density in each well was determined by quantifying the proteins after lysis using the PierceTM Micro BCATM assay kit. Bovine serum albumin in different diluted concentrations served as calibration curve. Adhesive and internalized NLCs were calculated in µg NLCs per mg protein.

2.7.4. In vitro cellular uptake

Since the method described above cannot differentiate between superficially attached and fully internalized NLCs, cellular uptake was additionally determined with a flow cytometer (BD LSRFortessa™ Cell sorter). Cellular uptake was evaluated as described above, with some modifications. NLCs were administered to cells in a concentration at 0.05% (*m/v*) in HBS. After removing the NLCs with ice-cold PBS, cells were detached from wells by incubating 150 µL of trypsin for 5 min at 37 °C on cells. As trypsin might harm cells within several minutes, its activity was stopped by the addition of 500 µL of MEM. The cell suspension was then separated into individual cells with a pipette for 30 s. To generate a measurable cell density, cells of two wells were combined into a 15 mL falcon tube. Cells were centrifuged at 800 rpm for four minutes. The supernatant was discarded and cell pellets were resuspended in PBS. To fully remove trypsin and MEM, the latter two steps were repeated twice. Subsequently, cells were filtered through a cell strainer with 70 µm pore size and diluted with PBS for flow cytometer analysis. LGR labeled NLCs internalized into cells were determined by measuring the fluorescence signal of > 10.000 events. To evaluate whether NLCs are fully internalized or only superficially attached, trypan blue was added to cell suspension at a concentration of 0.4% (*m/v*) to quench surface-bound nanocarriers (Knoll et al., 2022). Only viable single cells were considered by the gating strategy for further calculations. Results were expressed by cells that show high fluorescence after uptake of LGR labeled NLCs. All data were analyzed with FlowJo™v10.8.

2.7.5. Uptake mechanism

The uptake mechanism of NLCs through different endocytosis pathways was investigated using various endocytosis inhibitors. Therefore, Caco-2 cells were seeded on 24 well plates in a density of 2.5×10^4 cells per well and cultivated for two weeks. Cells were washed with HBS three times and then preincubated with the inhibitor for one hour. Uptake studies of 0.05% (*m/v*) NLCs were then conducted and determined by flow cytometer analysis as described above. Cells were exposed to the inhibitors throughout uptake studies. Caveolae-mediated endocytosis was inhibited by nystatin in a final concentration of 50 µM. Chlorpromazine at 10 µM served as an inhibitor of the clathrin-mediated endocytosis. Methyl-β-cyclodextrin (MβCD) was added at a concentration of 50 µM, at which it acts mainly as an inhibitor of caveolae-mediated endocytosis (Kazazic et al., 2006). To block the macropinocytosis, rottlerin was used in a concentration of 2 µM (Rusznyák et al., 2021). Caveolae- and clathrin-independent endocytosis was evaluated by the addition of quercetin at 20 µM (Wang et al., 2015). To investigate whether uptake only occurs by active transport, the study was conducted at 4 °C.

2.7.6. Thiol-dependent uptake

The effect of thiolated NLCs on cellular uptake by Caco-2 cells was investigated in an additional study that focused on cell surface thiols. As in the uptake mechanism study, cells were preincubated for one hour with reducing and oxidizing agents to form and cleave disulfide bonds on the cell surface. Glutathione (GSH) at 1 mM served as a reducing agent and hydrogen peroxide (H_2O_2) at the same concentration was used as an oxidizer. Both agents were also incubated with cells throughout the uptake studies of 0.05% (*m/v*) NLCs. NLCs were tested for size stability in the presence of these agents in a 24-hour preliminary study as shown in Figure S2. In addition, cytotoxicity of the reducing and oxidizing agents was examined as depicted in Figure S3. Cellular uptake was measured by a flow cytometer and analyzed with FlowJo™v10.8.

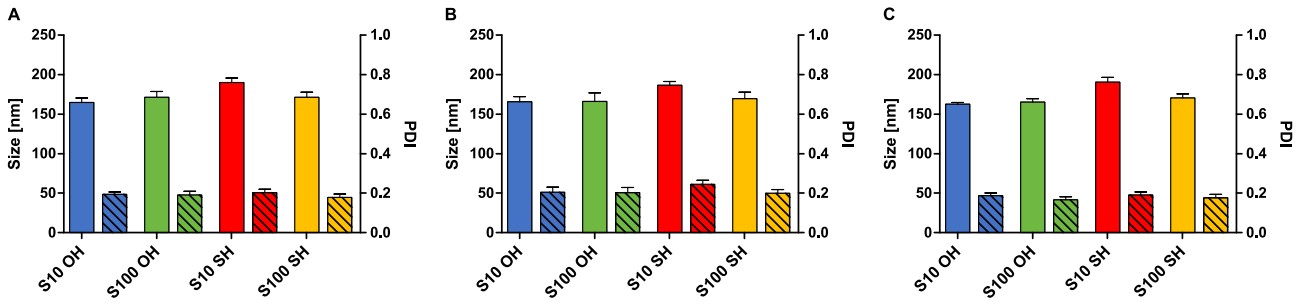

Fig. 1. Size (bars) and polydispersity index (hatched bars) of NLCs diluted 1:20 with demineralized water immediately after preparation (A), after 24 h under continuous shaking at 300 rpm at 37 °C (B), and after six months storage at 4 °C (C). Data are means of three experiments ± standard deviation.

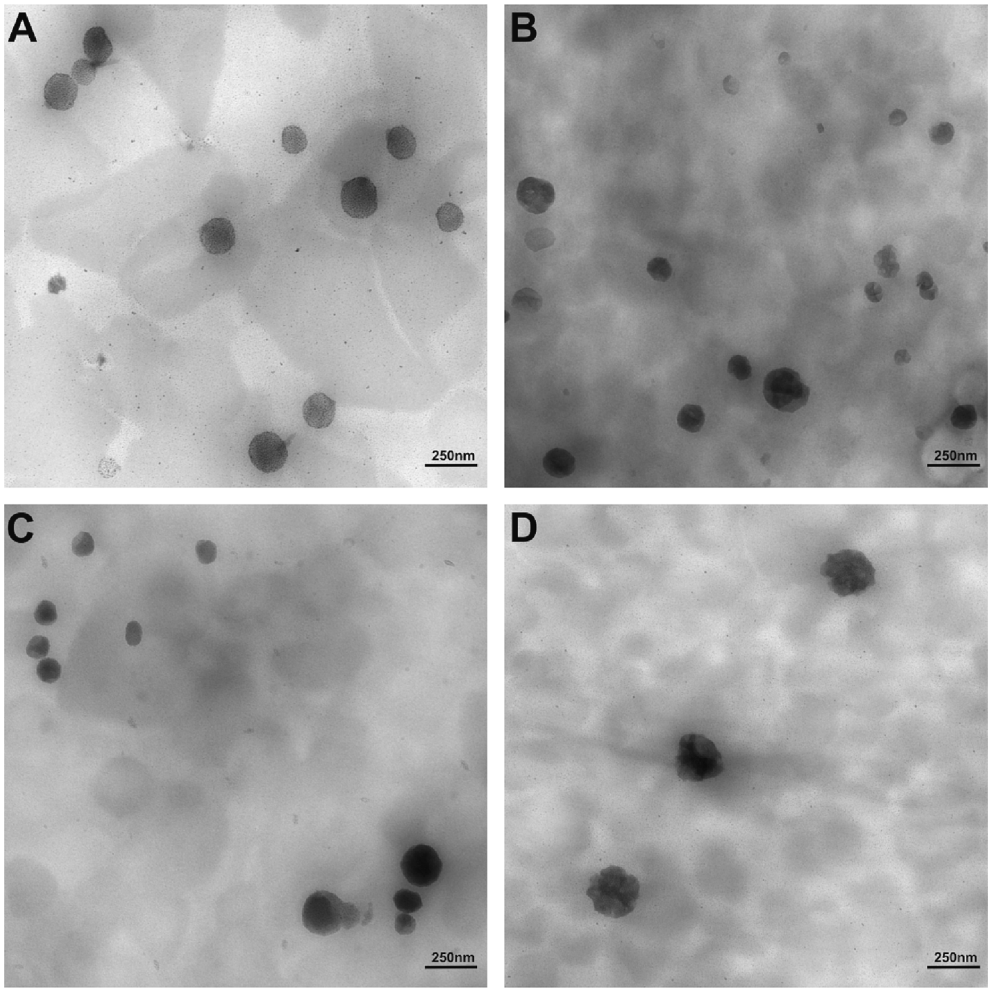

Fig. 2. EFTEM images of NLCs-PEG$_{10}$-OH (A), NLCs-PEG$_{100}$-OH (B), NLCs-PEG$_{10}$-SH (C) and NLCs-PEG$_{100}$-SH (D).

2.8. Statistical data analysis

Statistical data was analyzed with Graphpad Prism 5.01. Means of more groups were compared via one-way ANOVA and Bonferroni post-test. Two-way ANOVA with Bonferroni post-test was used to compare measurements repeated at multiple time points. The minimum level of significance was set at $p < 0.05$.

3. Results

3.1. Thiolation of surfactants

By the disulfide test the total amount of thiols was determined after reduction of the compounds, whereas by the Ellman's test the free unoxidized thiols were detected. For S10 SH the total amount of thiols was 800.8 μmol/g and 229.8 μmol/g free thiols were measured. S100 SH showed 425.4 μmol/g total thiols and 127.8 μmol/g unoxidized thiols.

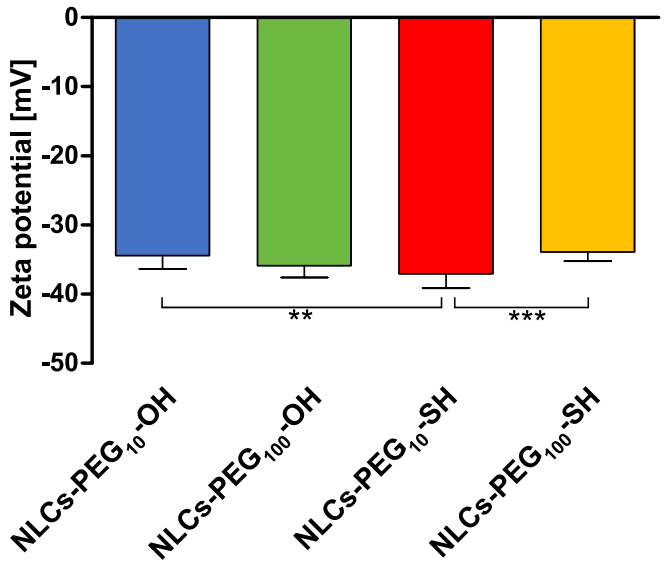

Fig. 3. Zeta potential of NLCs diluted 1:20 with demineralized water. Data are means of three experiments ± standard deviation. ** $p < 0.01$; *** $p < 0.001$.

3.2. Characterization of NLCs

Thiolated and unthiolated NLCs were prepared by a solvent evaporation method combined with ultrasonication. As shown in Fig. 1A all nanocarriers were prepared with a size below 200 nm. NLCs displayed no significant differences in their PDI. Furthermore, NLCs retained stable during storage over 24 h at 37 °C and six months at 4 °C as indicated in Fig. 1B and Fig. 1C. Results of DLS were additionally confirmed by EFTEM images as shown in Fig. 2. NLCs exhibited a spherical and homogenous shape without agglomeration. The results of zeta potential determinations are shown in Fig. 3. All NLCs displayed a negative zeta potential < -30 mV.

3.3. Evaluation of saquinavir loaded NLCs

Loading of SQV into NLCs led to stable nanocarriers as depicted in Table 1. No notable deviations in size, PDI and zeta potential compared to the unloaded NLCs were observed. Furthermore, drug loading and encapsulation efficiency did not differ significantly among these nanocarriers.

3.4. Cytotoxicity

NLCs were evaluated for their cytotoxic effects on Caco-2 cells at concentrations ranging from 0.01% to 2% (*m/v*) as displayed in Fig. 4A. At a concentration of 0.05% (*m/v*) of all nanocarriers, cells showed a viability over 80%. Therefore, this concentration is considered safe and further cell studies were performed at this concentration. First

Table 2
IC_{50} values of NLCs in % (*m/v*) determined by resazurin assay. Indicated values are means ± standard of three experiments. * $p < 0.05$ compared with NLCs-PEG_{100}-SH.

	PEG chain	NLCs	IC_{50}
Unthiolated	Short PEG chain	NLCs-PEG_{10}-OH	0.331 ± 0.106
	Long PEG chain	NLCs-PEG_{100}-OH	0.463 ± 0.036
Thiolated	Short PEG chain	NLCs-PEG_{10}-SH	0.269 ± 0.004*
	Long PEG chain	NLCs-PEG_{100}-SH	0.476 ± 0.058

Table 1
Determination of size, PDI, zeta potential, drug loading and encapsulations efficiency of SQV loaded NLCs. Indicated data are means of three experiments ± standard deviation.

NLCs	Size [nm]	PDI	Zeta potential [mV]	Drug loading [μg/mg]	Encapsulation efficiency [%]
NLCs-PEG_{10}-OH	161.5 ± 5.5	0.17 ± 0.01	−28.3 ± 0.6	21.60 ± 0.02	98.59 ± 0.15
NLCs-PEG_{100}-OH	171.3 ± 3.6	0.18 ± 0.01	−31.7 ± 0.5	21.56 ± 0.01	98.42 ± 0.09
NLCs-PEG_{10}-SH	199.7 ± 1.1	0.20 ± 0.01	−32.5 ± 0.3	21.53 ± 0.04	98.16 ± 0.12
NLCs-PEG_{100}-SH	172.0 ± 4.9	0.19 ± 0.02	−30.8 ± 0.5	21.56 ± 0.01	98.41 ± 0.09

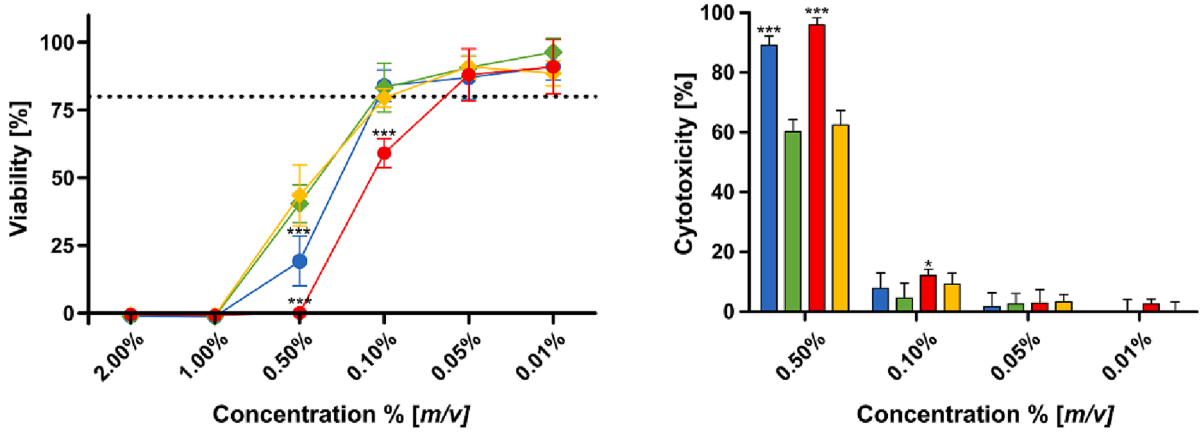

Fig. 4. (A) Viability of Caco-2 cells after treatment with NLCs-PEG_{10}-OH (blue), NLCs-PEG_{100}-OH (green), NLCs-PEG_{10}-SH (red) and NLCs-PEG_{100}-SH (orange) at indicated concentrations for 4 h determined by resazurin assay. 0.1% (*v/v*) Triton-X 100 served as positive control. Dotted line at 80% indicates cytocompatibility limit. Data are means of three experiments ± standard deviation. *** $p < 0.001$ compared with all other NLCs at the same concentration. (B) Cytotoxicity of Caco-2 cells after treatment with NLCs-PEG_{10}-OH (blue), NLCs-PEG_{100}-OH (green), NLCs-PEG_{10}-SH (red) and NLCs-PEG_{100}-SH (orange) at indicated concentrations for 12 h and determined by an LDH release assay. Data are means of three experiments ± standard deviation. *** $p < 0.001$ compared with NLCs-PEG_{100}-OH and NLCs-PEG_{100}-SH at the same concentration, * $p < 0.05$ compared with NLCs-PEG_{100}-OH.

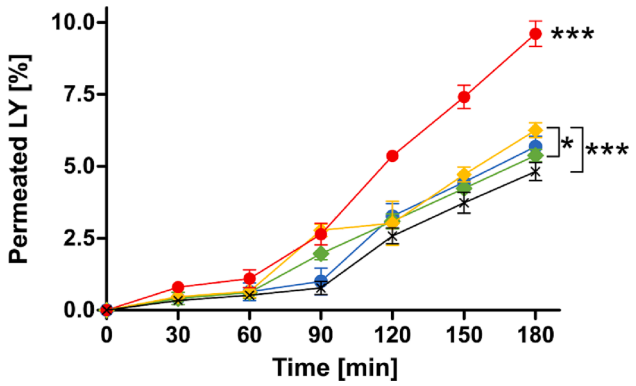

Fig. 5. Permeation of 0.1% (*m/v*) lucifer yellow (black) across Caco-2 cells at indicated time points during treatment with 0.05% (*m/v*) NLCs-PEG$_{10}$-OH (blue), NLCs-PEG$_{100}$-OH (green), NLCs-PEG$_{10}$-SH (red) and NLCs-PEG$_{100}$-SH (orange). Indicated values are means ± standard of three experiments. * $p < 0.05$; *** $p < 0.001$ compared with all other bars (NLCs-PEG$_{10}$-OH) or indicated other bars.

Table 3
P_{app} values of 0.1% (*m/v*) lucifer yellow (LY) across Caco-2 cell monolayer after 3 h incubation with 0.05% (*m/v*) of NLCs. Indicated values are means ± standard of three experiments. * $p < 0.05$ compared with LY, NLCs-PEG$_{10}$-OH and NLCs-PEG$_{100}$-OH; ** $p < 0.01$ compared with LY.

NLCs	$P_{app} \times 10^{-6}$ (cm/s)		Enhancement ratio
	Mean	SD	
LY	2.23	0.65	1
NLCs-PEG$_{10}$-OH	2.54	0.72	1.14
NLCs-PEG$_{100}$-OH	2.35	0.44	1.06
NLCs-PEG$_{10}$-SH	4.51$^{*/**}$	0.90	2.03*
NLCs-PEG$_{100}$-SH	3.15	0.53	1.42

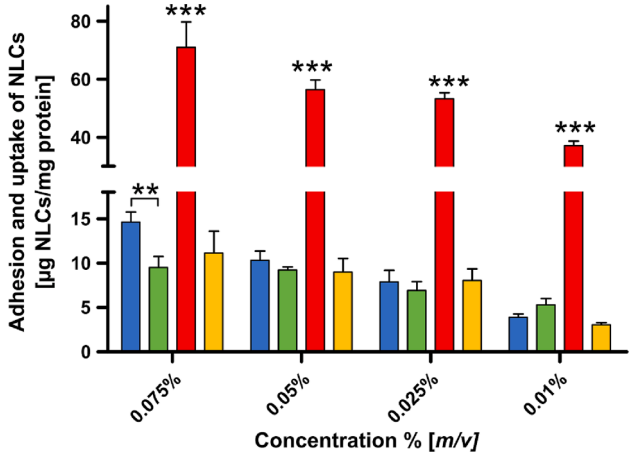

Fig. 6. Adhesion to the cell surface and internalization of Lumogen red labeled NLCs-PEG$_{10}$-OH (blue), NLCs-PEG$_{100}$-OH (green), NLCs-PEG$_{10}$-SH (red) and NLCs-PEG$_{100}$-SH (orange) at indicated concentrations after incubation for 3 h on cells at 37 °C. Cellular uptake determined in relation to protein content. Shown data are means of three experiments ± standard deviation. ** $p < 0.01$; *** $p < 0.001$ compared with all other bars.

significant cytotoxic effects were observed for the NLCs-PEG$_{10}$-SH at 0.1% (*m/v*). Moreover, higher toxicity of NLCs containing surfactants with shorter PEG chains was found. At a concentration of 0.5% (*m/v*) NLCs-PEG$_{10}$-OH and NLCs-PEG$_{10}$-SH showed significantly higher toxicity than NLCs-PEG$_{100}$-OH and NLCs-PEG$_{100}$-SH. IC_{50} values, displayed in Table 2, decreased in the following rank order: NLCs-PEG$_{100}$-SH > NLCs-PEG$_{100}$-OH > NLCs-PEG$_{10}$-OH > NLCs-PEG$_{10}$-SH.

In addition to the resazurin assay, an LDH release assay was performed to investigate the impact of nanocarriers on membrane integrity. High interactions of NLCs with the cell membrane can lead to membrane leakage and cell death. Cytotoxicity causes a release of LDH from the cytosol to the extracellular space. As shown in Fig. 4B, NLCs were not toxic at lower concentrations. In agreement with the results obtained by the resazurin assay NLCs-PEG$_{10}$-SH showed the highest cytotoxicity which was at 0.1% (*m/v*) significantly higher than that of NLCs-PEG$_{100}$-OH. Concentrations higher than 0.5% (*m/v*) could not be measured due to the high turbidity of the highly concentrated NLCs.

3.5. Permeation across Caco-2 cell monolayer

In addition to cellular uptake pathways, the effect of NLCs on the diffusion of LY across a Caco-2 cell monolayer was investigated. The permeation behaviour of LY in the presence of NLCs is shown in Fig. 5. Unthiolated NLCs showed only a slight increase in permeation of LY after 3 h, whereas thiolated NLCs significantly enhanced its permeation. In particular, NLCs-PEG$_{10}$-SH significantly enhanced permeation compared to all other NLCs. The permeation of LY was also significantly increased by NLCs-PEG$_{100}$-SH compared to NLCs-PEG$_{100}$-OH. The differences in permeation enhancement of LY are more evident from the calculated P_{app} values listed in Table 3, that shows increasing permeability of LY in the rank order: without NLCs < NLCs-PEG$_{100}$-OH < NLCs-PEG$_{10}$-OH < NLCs-PEG$_{100}$-SH < NLCs-PEG$_{10}$-SH. With an enhancement ratio of 2.03, NLCs-PEG$_{10}$-SH increased the P_{app} value of LY the most.

3.6. Adhesion to the cell surface and internalization of NLCs

Adhesion to the cell surface and internalization of thiolated and unthiolated NLCs was investigated using a Caco-2 cell line. As shown in Fig. 6, NLCs were allowed to interact with cells in concentrations ranging from 0.01% to 0.075% (*m/v*) for three hours. NLCs were prepared with 0.5% (*m/v*) LGR loading to allow quantification of the nanocarriers after administration to the cells. According to the results, NLCs-PEG$_{10}$-SH showed significantly increased cellular adhesion and internalization compared to all other NLCs at each concentration. At a concentration of 0.01% (*m/v*) adhesion and uptake of NLCs-PEG$_{10}$-SH was even 9.5-fold higher than that of NLCs-PEG$_{10}$-OH. Furthermore, NLCs-PEG$_{10}$-OH showed significantly higher cell adhesion and uptake at the highest concentration compared to NLCs-PEG$_{100}$-OH, demonstrating the superiority of the shorter PEG chains.

3.7. Cellular uptake

Since cell adhesion studies and internalization studies do not allow to distinguish between adhesive NLCs, that are only superficially bound to the cell membrane, and fully internalized NLCs, cellular uptake was also determined using a flow cytometer. Instead of lysing cells before measurement, cells were separated into individual cells and the fluorescence intensity of each cell was determined by a flow cytometer. To quench the signal of surface-bound NLCs, trypan blue was added before the analysis (Srivastava et al., 2011; Van Amersfoort and Van Strijp, 1994). The results presented in Fig. 7A show a significantly increased internalization of NLCs-PEG$_{10}$-SH compared with all other NLCs. In relation to NLCs-PEG$_{10}$-OH, the uptake with and without trypan blue quenching was 2.2 and 1.9 times higher, respectively. The 4.3-fold higher cellular uptake of NLCs-PEG$_{10}$-SH and the 2.0-fold higher uptake of NLCs-PEG$_{10}$-OH compared with NLCs-PEG$_{100}$-SH without quenching confirmed the results of the uptake study described above. The difference in uptake efficiency is also evident in the shift in fluorescence intensity without (Fig. 7B) and with trypan blue quenching (Fig. 7C), indicating a broader peak shifted to the right for NLCs-PEG$_{10}$-SH.

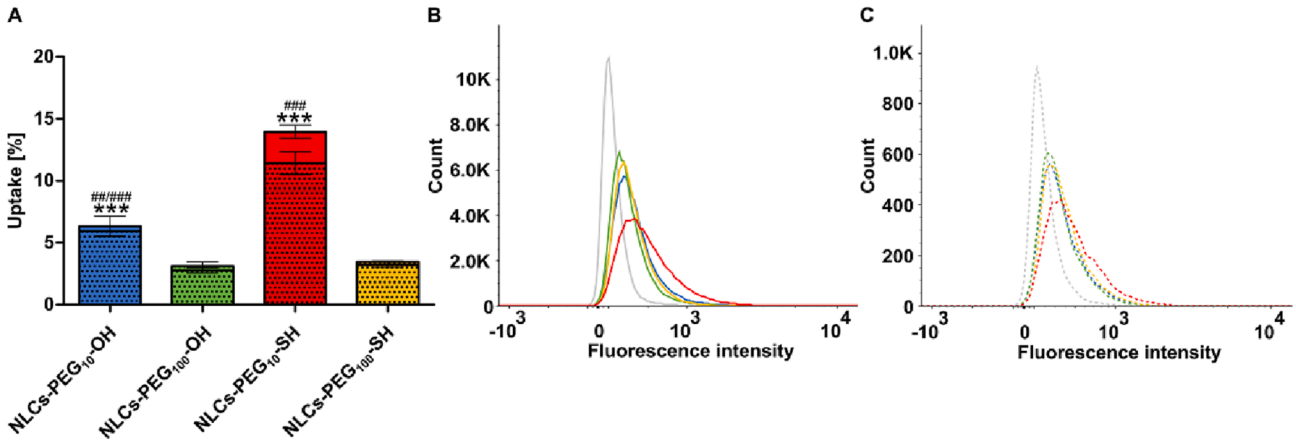

Fig. 7. (A) Percentage of cells showing a fluorescence signal after cellular uptake of Lumogen red labeled NLCs incubated on cells at a concentration of 0.05% (*m/v*) for 3 h. Undotted bars are without and dotted bars with trypan blue treatment. Indicated data are means of at least 3 experiments ± standard deviation. *** $p < 0.001$ compared to all other bars without trypan blue quenching. ## $p < 0.01$ compared with NLCs-PEG$_{100}$-SH with trypan blue treatment; ### $p < 0.001$ compared to all other bars with trypan blue treatment. Fluorescence intensity shift of cells incubated with buffer (grey), NLCs-PEG$_{10}$-OH (blue), NLCs-PEG$_{100}$-OH (green), NLCs-PEG$_{10}$-SH (red) and NLCs-PEG$_{100}$-SH (orange) without trypan blue (B) and with trypan blue quenching (C).

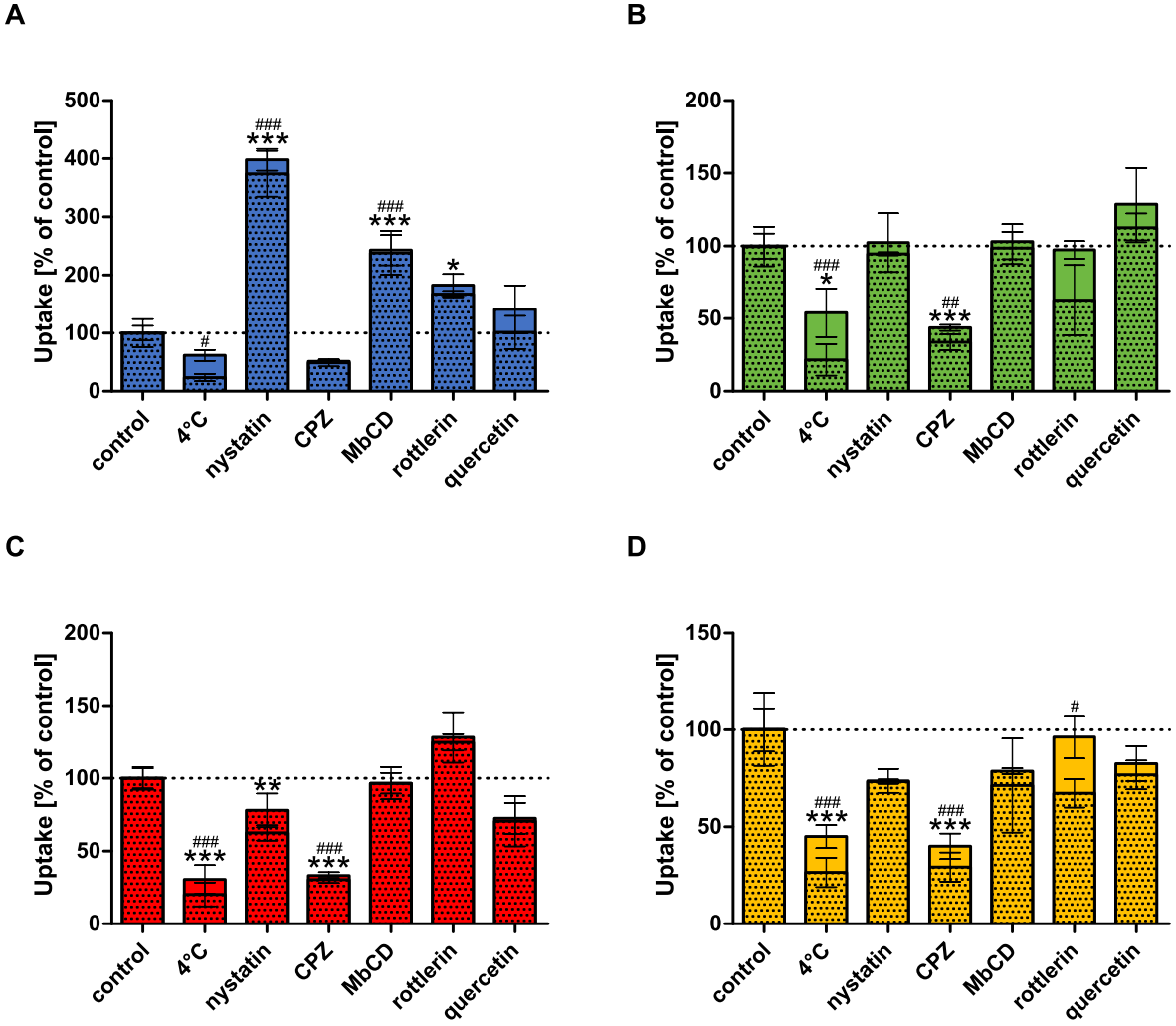

Fig. 8. Percentage of cells showing a fluorescence signal after cellular uptake of Lumogen red labeled NLCs-PEG$_{10}$-OH (A), NLCs-PEG$_{100}$-OH (B), NLCs-PEG$_{10}$-SH (C) and NLCs-PEG$_{100}$-SH (D) NLCs incubated on cells at a concentration of 0.05% (*m/v*) for 3 h. Cells were treated with inhibitors one hour before and during the uptake study. Undotted bars are without and dotted bars with trypan blue quenching. Indicated data are means of at least 3 experiments ± standard deviation. * $p < 0.05$; ** $p < 0.01$; *** $p < 0.001$ compared to the control (uptake at 37 °C) bar without trypan blue treatment. # $p < 0.05$; ## $p < 0.01$; ### $p < 0.001$ compared to the control bar with trypan blue treatment.

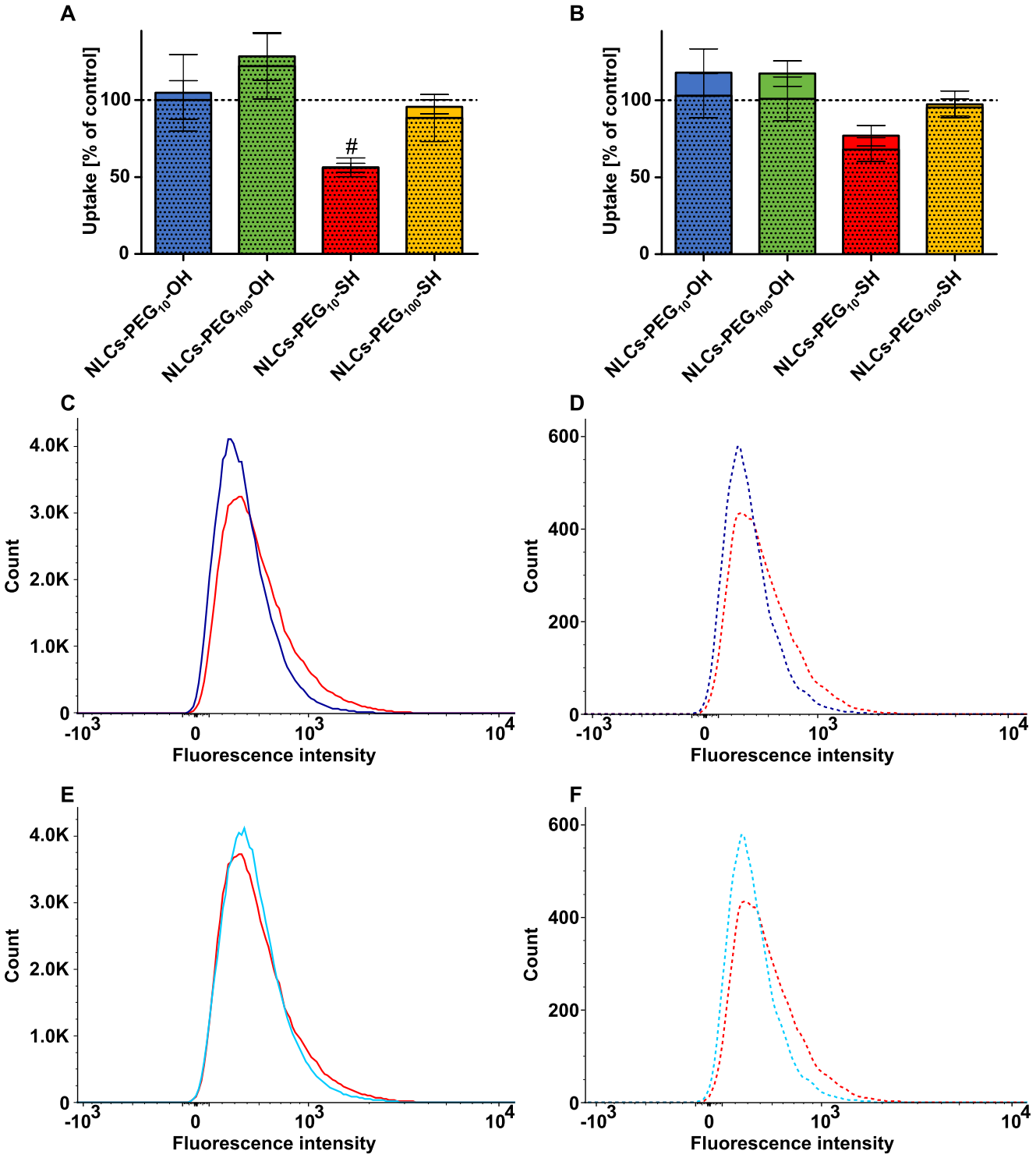

Fig. 9. Percentage of cells showing a fluorescence signal after cellular uptake of Lumogen red labeled NLCs-PEG$_{10}$-OH, NLCs-PEG$_{100}$-OH, NLCs-PEG$_{10}$-SH and NLCs-PEG$_{100}$-SH incubated on cells at a concentration of 0.05% (*m/v*) for 3 h. Cells were treated with H_2O_2 (A) and GSH (B) one hour before and during the uptake study. Undotted bars are without and dotted bars with trypan blue treatment. Indicated data are means of three experiments ± standard deviation. # $p < 0.05$ compared to the control bar with trypan blue treatment. Fluorescence intensity shift of NLCs-PEG$_{10}$-SH (red) incubated on H_2O_2 (purple) treated cells without trypan blue quenching (C) and with trypan blue quenching (D). Fluorescence intensity shift of NLCs-PEG$_{10}$-SH incubated on GSH (light blue) treated cells without trypan blue quenching (E) and with trypan blue quenching (F).

3.8. Uptake mechanism

The underlying uptake mechanism of NLCs was investigated in the presence of various endocytosis inhibitors and at 4 °C. According to the results shown in Fig. 8 uptake of all nanocarriers was significantly inhibited at 4 °C. In addition, uptake of all nanocarriers was lowered to >50% by CPZ. Nystatin, MβCD and rottlerin increased the uptake of NLCs-PEG$_{10}$-OH significantly. An enhancement was also observed with quercetin for the unthiolated NLCs. In contrast to the unthiolated NLCs, nystatin caused a decrease in uptake in thiolated NLCs that was significant in NLCs-PEG$_{10}$-SH. The same was observed for quercetin, lowering the uptake of NLCs-PEG$_{10}$-SH and NLCs-PEG$_{100}$-SH to 70.5% and 76.8%, respectively. Rottlerin affected the uptake of NLCs with long PEG chains, being significant for NLCs-PEG$_{100}$-SH.

3.9. Thiol-dependent uptake

The mechanism of cellular uptake of thiolated nanocarriers has not yet been fully understood. So far, mainly the uptake of thiolated peptides was studied, but not that of NLCs. To further deepen our knowledge of the underlying mechanism, thiol-dependent uptake was investigated by use of an oxidizing and reducing agent. As shown in Fig. 9A and Fig. 9B, cellular uptake of unthiolated NLCs was not significant influenced by H_2O_2 and GSH, whereas uptake of NLCs-PEG$_{10}$-SH was decreased. In particular, H_2O_2 significantly lowered to 56% the uptake after trypan blue quenching. Inhibition of uptake is also highlighted by the shift in fluorescence intensity to a sharp peak at lower values, as illustrated in Fig. 9C and Fig. 9D after trypan blue quenching. By addition of GSH the uptake was less decreased to 68%, as shown in Fig. 9E and Fig. 9F after trypan blue quenching.

4. Discussion

4.1. Characterization of NLCs

NLCs were obtained in a size below 200 nm according to the results of DLS and EFTEM, which is advantageous for cellular uptake. According to Kulkarni et al., cellular uptake decreases for nanocarriers >200 nm (Kulkarni and Feng, 2013). The NLCs-PEG$_{10}$-SH exhibit a slightly larger particle size, that could be attributed to disulfide bond formations by the thiolated surfactant. The shape of NLCs with short PEG chains appeared to be more spherical and homogeneous than that of NLCs with long PEG chains. This observation can be attributed to the PEG brush of the long PEG chains, which is the only difference to NLCs with short PEG chains.

Thiolation of the short PEG chain surfactant led to NLCs with a slightly lower zeta potential. This observation might be explained by the thiolate anion, which can be formed in aqueous media at neutral pH. Thielbeer et al. described the changes in zeta potential of nanocarriers after modification of their surface chemistry (Thielbeer et al., 2011). Similar to the results shown, thiolation resulted in a shift towards a more negative surface charge. This effect could not be observed for NLCs bearing the longer thiolated polyethylene glycol (PEG) chains in form of the S100 SH. Since the flexible long PEG chains tend to occur in a brush conformation, the terminal thiol groups may be hidden inside this brush being therefore not available on the surface (Friedl et al., 2021). In contrast, short PEG chains are elongated so that the thiol group points outwards.

Loading of SQV resulted in stable NLCs that were not significantly different in size, PDI, and zeta potential to unloaded NLCs. The high encapsulation efficiency was confirmed by almost no detectable SQV outside the lipid matrix of the nanocarriers.

4.2. Cytotoxicity studies

The NLCs-PEG$_{10}$-SH showed in both cytotoxicity studies the highest impact on cell viability. A reason for this higher toxicity could be the stronger interactions of NLCs with the cell membrane due to the formation of disulfide bonds between cellular and nanocarrier thiols. Ujhelyi et al. investigated the cytotoxic effect of different surfactants on Caco-2 cells (Ujhelyi et al., 2012). Cytotoxicity was found to be influenced by the concentration and modification of the surfactant. Increasing interactions with the lipids of the cell membrane lead to membrane destabilization, culminating in cell lysis. Since the content of surfactant is equal in all applied NLCs, the main cause for higher cytotoxicity is likely the modification of the surfactant by thiolation. The overall higher toxic effects of NLCs with shorter PEG chain surfactants matches with results obtained by Ekelund et al. demonstrating decreasing toxicity against Caco-2 cells with increasing chain length of PEG (Ekelund et al., 2005). Since no pronounced differences were observed between the thiolated and the non-thiolated NLCs-PEG$_{100}$, it can be assumed that the terminal thiols are hidden inside the PEG brush.

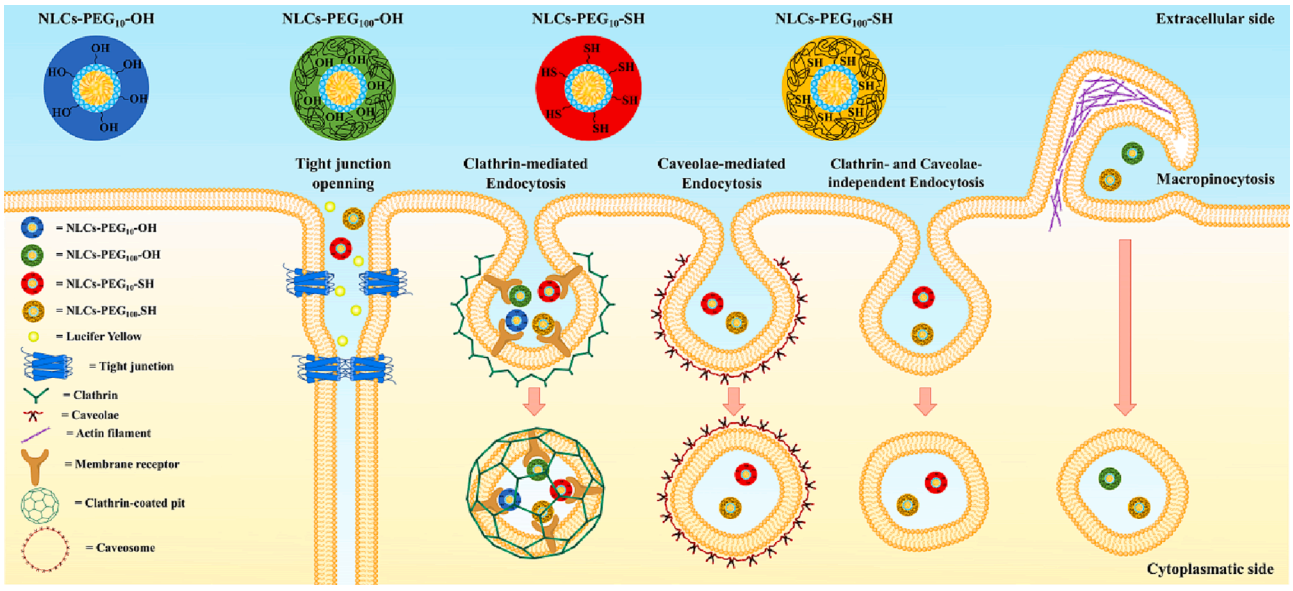

Fig. 10. Schematic illustration of endocytosis mechanisms and opening of tight junctions by NLCs. For each interaction mechanism, NLCs were indicated that had shown the greatest impact.

The significantly different IC50 values of NLCs-PEG_{10}-SH and NLCs-PEG_{100}-SH suggest that the length of the PEG chain and the availability of thiols on the surface of the NLCs might have the greatest influence on cytotoxicity.

4.3. Cellular interaction studies

The thiolated NLCs enhanced permeation of LY to a higher extent than the unthiolated NLCs. This observation can be explained by the ability of thiols to open tight junctions between cells, thereby increasing permeability through the Caco-2 cell layer (Hock et al., 2022). The opening of tight junction by thiolated NLCs is illustrated in Fig. 10. The results are consistent with previous studies describing increased permeability of sodium fluorescein and fluorescein isothiocyanate-dextran due to opening of tight junctions by thiols (Perera et al., 2011). NLCs-PEG_{10}-SH showed the highest increase in permeation of LY, which can be attributed to the high capability of the short thiolated PEG chains to open tight junctions. In comparison, NLCs-PEG_{100}-SH showed less permeation enhancement than NLCs-PEG_{10}-SH, which can be explained by the lower number of thiols on the surface of NLCs-PEG_{100}-SH. Due to the higher molecular weight of S100 SH, less thiolated surfactant molecules cover the surface of these NLCs. Unfortunately, the same molarity of surfactants in the short and long PEG chain NLCs could not be applied to form stable NLCs without micelles formation (Beloqui et al., 2016; Pezeshki et al., 2019). In addition, some thiols of the long-chain PEG might be available on the surface of NLCs to open the tight junctions, but their concentration is too low to cause a pronounced effect.

NLCs-PEG_{10}-SH showed the highest interaction with cells. This observation is in agreement with results of cytotoxicity studies showing enhanced interactions between the NLCs-PEG_{10}-SH and Caco-2 cells. Fröhlich provided evidence for the correlation between enhanced cytotoxicity and enhanced cellular uptake of positively charged nanocarriers (Fröhlich, 2012). She cited higher interactions of the nanocarrier with the cell membrane as the reason for this. The same could apply to NLCs-PEG_{10}-SH. Since the investigated NLCs showed no positive surface charge, thiols have to be involved in the uptake mechanism. The formation of disulfide bonds between the cell surface and NLCs seems to be a plausible explanation. The cell surface is covered with various exofacial proteins and enzymes such as integrins, scavenger receptors and protein tyrosine phosphatase, exhibiting cysteine-rich domains that can form disulfide bonds with the thiols of NLCs-PEG_{10}-SH (Laurent et al., 2021; Leichner et al., 2019). Similar to results obtained in the cytotoxicity study, the long-chain NLCs-PEG_{100}-OH and NLCs-PEG_{100}-SH showed no significant difference in uptake. This observation might be explained by the lower number of thiols and by the shielding effect of the PEG corona formed by a long PEG chain recently described by our research group (Friedl et al., 2020). The PEG corona can reduce cellular uptake, firstly by providing a steric hindrance and secondly by reducing the electrostatic interactions between the cells and the nanocarriers. Therefore, uptake might be mainly influenced by the thiolation of short PEG chains and also by the chain length of the PEG surfactant.

Since thiolated and unthiolated NLCs differed markedly in their cellular uptake efficiency, the underlying uptake mechanism was investigated to deepen the basic understanding of how thiols affect the mode of internalization. Therefore, cellular uptake studies were performed with different endocytosis inhibitors and at low temperature. The decrease in uptake at 4 °C after trypan blue quenching indicates that the nanocarriers are only bound to the surface of cells and were not internalized due to the inhibition of the ATP-dependent transport (Nagai et al., 2019). Nystatin treatment of cells inhibits caveolae-mediated endocytosis (He et al., 2013). Nanocarriers that are internalized by this endocytic pathway tend to escape endosomes and the degradation in lysosomes (Behzadi et al., 2017). Nystatin did not inhibit the uptake of unthiolated NLCs, indicating that there is no endocytosis by caveolae. On the contrary, the uptake of NLCs-PEG_{10}-OH was markedly increased even after trypan blue treatment. This increase in uptake might be caused by the overcompensation and upregulation of alternative endocytosis pathways, described in the literature by various research groups (Beloqui et al., 2013; Hufnagel et al., 2009; Vercauteren et al., 2010). The inhibition of uptake of thiolated NLCs by nystatin indicated involvement of caveolae-mediated uptake by thiolation. A possible relationship between the caveolae invaginations and thiols was also mentioned by Yamabhai et al., who indicated a dependence of the transport of endothelial growth factor to caveolae on the cysteine-rich region (Yamabhai and Anderson, 2002). Furthermore, endocytosis of unthiolated and thiolated NLCs appeared to be clathrin-mediated, as the uptake of all nanocarriers was decreased by CPZ, an inhibitor of clathrin-mediated endocytosis. MβCD, an inhibitor of caveolae-mediated endocytosis, had no effect on NLCs-PEG_{100}-OH and thiolated NLCs but significantly increased the uptake of NLCs-PEG_{10}-OH. This observation is consistent with the increased uptake obtained by nystatin. Similar to nystatin, the increased uptake could be caused by upregulation of alternative endocytosis pathways. The macropinocytosis inhibitor rottlerin caused an increased uptake of NLCs-PEG_{10}-OH and NLCs-PEG_{10}-SH, whereas the uptake of NLCs-PEG_{100}-OH and NLCs-PEG_{100}-SH was lowered. The chain length of tested PEG surfactants might therefore have an influence on macropinocytosis. The short-chain PEG surfactants triggered the upregulation of other endocytosis pathways, which was not observed with the long-chain PEG. As at 4 °C, rottlerin caused a pronounced difference in surface-attached and fully internalized NLCs-PEG_{100}-OH and NLCs-PEG_{100}-SH after trypan blue quenching. In case of quercetin, an inhibitor of the caveolae- and clathrin-independent endocytosis, no effect was observed for the unthiolated NLCs, whereas the uptake of thiolated NLCs was decreased. According to these results, thiolation causes a shift in the uptake pathway towards caveolae- and clathrin-independent and caveolae-mediated internalization. Thiol-dependent uptake might be related to these two endocytosis pathways. Direct comparison of NLCs-PEG10-SH with NLCs-PEG100-SH showed that the availability of thiols on the NLC surface did not significantly affect the mechanism but the extent of uptake. Different endocytosis mechanisms of NLCs were illustrated schematically in Fig. 10.

The different uptake mechanisms of thiolated and non-thiolated NLCs were additionally investigated with oxidizing and reducing agents to confirm the thiol dependence of the internalization process H_2O_2 and GSH did not affect the uptake of unthiolated NLCs, since no thiols were available on the surface of NLCs. Oxidation and reduction of membrane bound thiols seems to be irrelevant for the uptake of the unthiolated NLCs, since no interactions can occur. In contrast, the oxidizing agent H_2O_2 lowered the uptake of NLCs-PEG_{10}-SH. Torres et al. described three conjectures for the mechanism of thiol-dependent uptake by transmembrane thiolated proteins, which are internalized after disulfide bond formation with the administered thiolated biomolecule (Torres and Gait, 2012). Accordingly, uptake may occur after formation of a disulfide bond between a disulfide group of the nanocarrier and an exofacial thiol or an exofacial disulfide group on the cell membrane and a thiol of the nanocarrier. The third mechanism, which is only poorly understood, describes the formation of disulfide bonds between two reduced thiols on the cell membrane and on the nanocarrier enabled by metal ions. The decreased uptake after incubation with H_2O_2 might be explained by intramolecular disulfide bond formations of the thiols of the nanocarriers itself as well thiols of transmembrane proteins. Since disulfide exchange reactions between two disulfides can be excluded due to the missing thiolate nucleophile (Fernandes and Ramos, 2004), disulfides of transmembrane proteins and disulfides of the nanocarrier cannot interact with each other. By addition of GSH the uptake was less decreased. Incubation of NLCs with GSH on cells led to a reduction of membrane bound thiols and thiols on the nanocarriers. Disulfide formation between reduced thiols would only follow the third mechanism mentioned above and uptake is hence decreased. Another

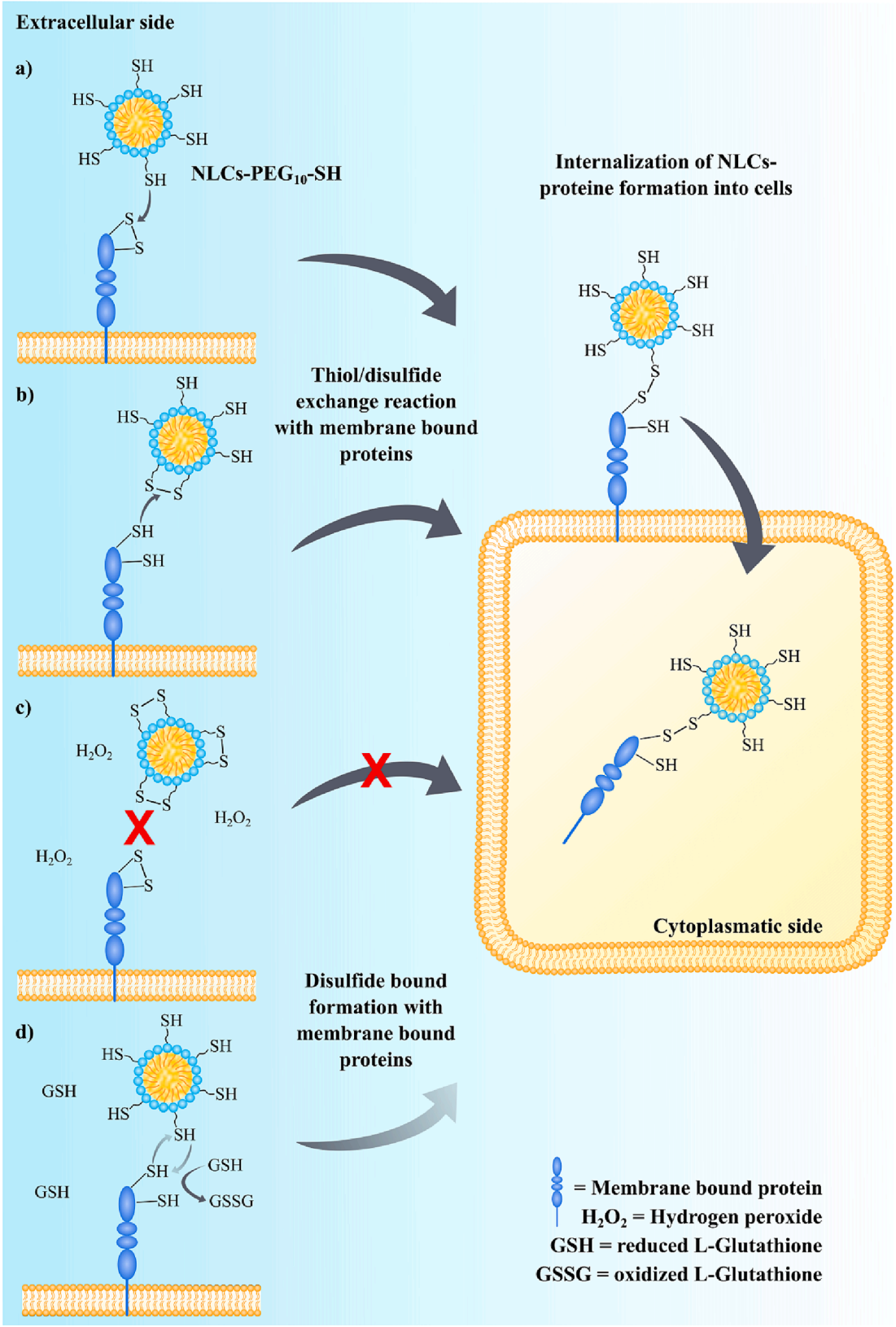

Fig. 11. Schematic illustration of thiol dependent cellular uptake of NLCs-PEG_{10}-SH via disulfide formation with thiols of membrane bound proteins. a) thiol/disulfide exchange reaction between thiol of NLCs and disulfide of membrane bound protein. b) thiol/disulfide exchange reaction between thiol of membrane bound protein and disulfide of NLCs. c) Oxidation of thiol by hydrogen peroxide impeding disulfide exchange reactions. d) reduction of disulfides resulting in less disulfide bond formations of NLCs with proteins.

plausible reason might be the cleavage of already formed disulfides between transmembrane proteins and the nanocarriers by GSH before internalization could take place. The possible disulfide bond formations of NLCs-PEG_{10}-SH with thiols of membrane bound proteins are illustrated in Fig. 11. Similar to the results of the cellular uptake study performed with NLCs alone, NLCs-PEG_{100}-SH showed only slight decrease when incubated with H_2O_2 and GSH, just like NLCs-PEG_{100}-OH. The reason for this observation might be the lower number of thiols on the surface of NLCs-PEG_{100}-SH and a limited access of these thiols due to the PEG brush preventing the interaction with thiols on the cell membrane.

5. Conclusion

Since lipid-based nanocarriers suffer from poor cellular uptake, different strategies were applied to address this shortcoming. A rather new approach is the surface decoration of the nanocarriers with thiols to initiate thiol-dependent uptake. Following this strategy, we prepared NLCs using a thiolated PEG surfactant that was anchored on their surface. Successful implementation of this resulted in an increased adhesion to the cell surface and internalization, that was in particular up to 9.5-fold higher for NLCs-PEG_{10}-SH compared to the unthiolated NLCs-PEG_{10}-OH. Short PEG chain NLCs, especially the thiolated, showed higher cellular uptake than NLCs with longer PEG chain. The longer PEG chains resulted in less availability of the terminal thiol for cell interactions. The uptake mechanism of all NLCs appeared to be through active transport, as uptake was significantly decreased at 4 °C. Use of endocytosis inhibitors demonstrated clathrin-mediated endocytosis of NLCs. Thiolated NLCs additionally indicated caveolae-dependent and clathrin- and caveolae-independent uptake. Macropinocytosis occurred only in NLCs bearing long PEG chains. Thiol-dependent uptake mechanism of NLCs-PEG_{10}-SH was verified by a reducing and oxidizing agent. Moreover, thiolated NLCs showed enhanced permeation of lucifer yellow across a Caco-2 cell monolayer. In conclusion, thiolation of NLCs results in multifunctional nanocarriers that exhibit enhanced cellular uptake due to various additional uptake mechanisms.

CRediT authorship contribution statement

Patrick Knoll: Conceptualization, Methodology, Investigation, Visualization, Writing – original draft, Writing – review & editing. **Giuseppe Francesco Racaniello:** Conceptualization, Methodology, Investigation. **Valentino Laquintana:** Conceptualization, Methodology, Investigation. **Florina Veider:** Methodology, Investigation. **Ahmad Saleh:** Methodology, Investigation. **Anna Seybold:** Conceptualization, Methodology, Investigation, Writing – review & editing. **Nunzio Denora:** Conceptualization, Writing – review & editing, Funding acquisition, Supervision. **Andreas Bernkop-Schnürch:** Conceptualization, Writing – review & editing, Funding acquisition, Supervision.

Declaration of Competing Interest

The authors declare that they have no known competing financial interests or personal relationships that could have appeared to influence the work reported in this paper.

Data availability

Data will be made available on request.

Funding

Ahmad Saleh was supported by the BPPLN scholarship scheme of the Ministry of Education, Culture, Research and Technology of The Republic of Indonesia.

Appendix A. Supplementary data

Supplementary data to this article can be found online at https://doi.org/10.1016/j.ijpharm.2023.122753.

References

Artursson, P., Palm, K., Luthman, K., 2012. Caco-2 monolayers in experimental and theoretical predictions of drug transport. Adv. Drug Deliv. Rev. 64, 280–289. https://doi.org/10.1016/j.addr.2012.09.005.

Behzadi, S., Serpooshan, V., Tao, W., Hamaly, M.A., Alkawareek, M.Y., Dreaden, E.C., Brown, D., Alkilany, A.M., Farokhzad, O.C., Mahmoudi, M., 2017. Cellular uptake of nanoparticles: Journey inside the cell. Chem. Soc. Rev. 46, 4218–4244. https://doi.org/10.1039/c6cs00636a.

Beloqui, A., Solinís, M.Á., Gascón, A.R., Del Pozo-Rodríguez, A., Des Rieux, A., Préat, V., 2013. Mechanism of transport of saquinavir-loaded nanostructured lipid carriers across the intestinal barrier. J. Control. Release 166, 115–123. https://doi.org/10.1016/j.jconrel.2012.12.021.

Beloqui, A., Solinís, M.Á., Rodríguez-Gascón, A., Almeida, A.J., Préat, V., 2016. Nanostructured lipid carriers: Promising drug delivery systems for future clinics. Nanomedicine Nanotechnology. Biol. Med. 12, 143–161. https://doi.org/10.1016/j.nano.2015.09.004.

Bhat, S.S., Mukherjee, D., Sukharamwala, P., Dehuri, R., Murali, A., Teja, B.V., 2021. Thiolated polymer nanocarrier reinforced with glycyrrhetinic acid for targeted delivery of 5-fluorouracil in hepatocellular carcinoma. Drug Deliv. Transl. Res. 11, 2252–2269. https://doi.org/10.1007/s13346-020-00894-2.

Bonengel, S., Bernkop-Schnürch, A., 2014. Thiomers - From bench to market. J. Control. Release 195, 120–129. https://doi.org/10.1016/j.jconrel.2014.06.047.

Ekelund, K., Östh, K., Påhlstorp, C., Björk, E., Ulvenlund, S., Johansson, F., 2005. Correlation between epithelial toxicity and surfactant structure as derived from the effects of polyethyleneoxide surfactants on Caco-2 cell monolayers and pig nasal mucosa. J. Pharm. Sci. 94, 730–744. https://doi.org/10.1002/jps.20283.

Fernandes, P.A., Ramos, M.J., 2004. Theoretical Insights into the Mechanism for Thiol/Disulfide Exchange. Chem. - A Eur. J. 10, 257–266. https://doi.org/10.1002/chem.200305343.

Friedl, J.D., Steinbring, C., Zaichik, S., Le, N.M.N., Bernkop-Schnürch, A., 2020. Cellular uptake of self-emulsifying drug-delivery systems: Polyethylene glycol versus polyglycerol surface. Nanomedicine 15, 1829–1841. https://doi.org/10.2217/nnm-2020-0127.

Friedl, J.D., Nele, V., De Rosa, G., Bernkop-Schnürch, A., 2021. Bioinert, Stealth or Interactive: How Surface Chemistry of Nanocarriers Determines Their Fate In Vivo. Adv. Funct. Mater. 31 https://doi.org/10.1002/adfm.202103347.

Fröhlich, E., 2012. The role of surface charge in cellular uptake and cytotoxicity of medical nanoparticles. Int. J. Nanomedicine 7, 5577–5591. https://doi.org/10.2147/IJN.S36111.

Gómez-Guillén, M.C., Montero, M.P., 2021. Enhancement of oral bioavailability of natural compounds and probiotics by mucoadhesive tailored biopolymer-based nanoparticles: A review. Food Hydrocoll. 118 https://doi.org/10.1016/j.foodhyd.2021.106772.

Grassiri, B., Knoll, P., Fabiano, A., Piras, A.M., Zambito, Y., Bernkop-schnürch, A., 2022. Thiolated Hydroxypropyl- β -cyclodextrin : A Potential Multifunctional Excipient for Ocular Drug Delivery.

He, B., Lin, P., Jia, Z., Du, W., Qu, W., Yuan, L., Dai, W., Zhang, H., Wang, X., Wang, J., Zhang, X., Zhang, Q., 2013. The transport mechanisms of polymer nanoparticles in Caco-2 epithelial cells. Biomaterials 34, 6082–6098. https://doi.org/10.1016/j.biomaterials.2013.04.053.

Hock, N., Racaniello, G.F., Aspinall, S., Denora, N., Khutoryanskiy, V.V., Bernkop-Schnürch, A., 2022. Thiolated Nanoparticles for Biomedical Applications: Mimicking the Workhorses of Our Body. Adv. Sci. 9, 1–24. https://doi.org/10.1002/advs.202102451.

Hufnagel, H., Hakim, P., Lima, A., Hollfelder, F., 2009. Fluid phase endocytosis contributes to transfection of DNA by PEI-25. Mol. Ther. 17, 1411–1417. https://doi.org/10.1038/mt.2009.121.

Irmukhametova, G.S., Mun, G.A., Khutoryanskiy, V.V., 2011. Thiolated mucoadhesive and PEGylated nonmucoadhesive organosilica nanoparticles from 3-mercaptopropyltrimethoxysilane. Langmuir 27, 9551–9556. https://doi.org/10.1021/la201385h.

Jalil, A., Asim, M.H., Nazir, I., Matuszczak, B., Bernkop-Schnürch, A., 2020. Self-emulsifying drug delivery systems containing hydrophobic ion pairs of polymyxin B and agaric acid: A decisive strategy for enhanced antimicrobial activity. J. Mol. Liq. 311, 113298 https://doi.org/10.1016/j.molliq.2020.113298.

Jiang, L., Li, X., Liu, L., Zhang, Q., 2013. Thiolated chitosan-modified PLA-PCL-TPGS nanoparticles for oral chemotherapy of lung cancer. Nanoscale Res. Lett. 8, 1–11. https://doi.org/10.1186/1556-276X-8-66.

Kali, G., Knoll, P., Bernkop-schnürch, A., 2022. Emerging technologies to increase gastrointestinal transit times of drug delivery systems. J. Control. Release 346, 289–299. https://doi.org/10.1016/j.jconrel.2022.04.016.

Kazazic, M., Roepstorff, K., Johannessen, L.E., Pedersen, N.M., van Deurs, B., Stang, E., Madshus, I.H., 2006. EGF-induced activation of the EGF receptor does not trigger mobilization of caveolae. Traffic 7, 1518–1527. https://doi.org/10.1111/j.1600-0854.2006.00487.x.

Knoll, P., Le, N.M.N., Wibel, R., Baus, R.A., Kali, G., Asim, M.H., Bernkop-Schnürch, A., 2021. Thiolated pectins: In vitro and ex vivo evaluation of three generations of thiomers. Acta Biomater. https://doi.org/10.1016/j.actbio.2021.08.016.

Knoll, P., Hörmann, N., Nguyen Le, N.M., Wibel, R., Gust, R., Bernkop-Schnürch, A., 2022. Charge converting nanostructured lipid carriers containing a cell-penetrating peptide for enhanced cellular uptake. J. Colloid Interface Sci. 628, 463–475. https://doi.org/10.1016/j.jcis.2022.07.160.

Kulkarni, S.A., Feng, S.S., 2013. Effects of particle size and surface modification on cellular uptake and biodistribution of polymeric nanoparticles for drug delivery. Pharm. Res. 30, 2512–2522. https://doi.org/10.1007/s11095-012-0958-3.

Laurent, Q., Martinent, R., Lim, B., Pham, A.-T., Kato, T., López-Andarias, J., Sakai, N., Matile, S., 2021. Thiol-Mediated Uptake. JACS Au 1, 710–728. https://doi.org/10.1021/jacsau.1c00128.

Leichner, C., Jelkmann, M., Bernkop-Schnürch, A., 2019. Thiolated polymers: Bioinspired polymers utilizing one of the most important bridging structures in nature. Adv. Drug Deliv. Rev. 152, 191–221. https://doi.org/10.1016/j.addr.2019.04.007.

Li, Z., Jiang, H., Xu, C., Gu, L., 2015. A review: Using nanoparticles to enhance absorption and bioavailability of phenolic phytochemicals. Food Hydrocoll. 43, 153–164. https://doi.org/10.1016/j.foodhyd.2014.05.010.

Meng, J., Zhang, T., Agrahari, V., Ezoulin, M.J., Youan, B.B.C., 2014. Comparative biophysical properties of tenofovir-loaded, thiolated and nonthiolated chitosan nanoparticles intended for HIV prevention. Nanomedicine 9, 1595–1612. https://doi.org/10.2217/nnm.13.136.

Muchow, M., Maincent, P., Müller, R.H., 2008. Lipid nanoparticles with a solid matrix (SLN®, NLC®, LDC®) for oral drug delivery. Drug Dev. Ind. Pharm. 34, 1394–1405. https://doi.org/10.1080/03639040802130061.

Nagai, N., Ogata, F., Otake, H., Nakazawa, Y., Kawasaki, N., 2019. Energy-dependent endocytosis is responsible for drug transcorneal penetration following the instillation of ophthalmic formulations containing indomethacin nanoparticles. Int. J. Nanomedicine 14, 1213–1227. https://doi.org/10.2147/IJN.S196681.

Perera, G., Barthelmes, J., Vetter, A., Krieg, C., Uhlschmied, C., Bonn, G.K., Bernkop-Schnürch, A., 2011. Thiolated polycarbophil/glutathione: Defining its potential as a permeation enhancer for oral drug administration in comparison to sodium caprate. Drug Deliv. 18, 415–423. https://doi.org/10.3109/10717544.2011.570807.

Pezeshki, A., Hamishehkar, H., Ghanbarzadeh, B., Fathollahy, I., Keivani Nahr, F., Khakbaz Heshmati, M., Mohammadi, M., 2019. Nanostructured lipid carriers as a favorable delivery system for β-carotene. Food Biosci. 27, 11–17. https://doi.org/10.1016/j.fbio.2018.11.004.

Racaniello, G.F., Knoll, P., Jörgensen, A.M., Arduino, I., Laquintana, V., Lopedota, A.A., Bernkop-Schnürch, A., Denora, N., 2022. Thiolation of non-ionic surfactants for the development of lipid-based mucoadhesive drug delivery systems. Eur. J. Pharm. Biopharm. 179, 95–104. https://doi.org/10.1016/j.ejpb.2022.08.015.

Rennick, J.J., Johnston, A.P.R., Parton, R.G., 2021. Key principles and methods for studying the endocytosis of biological and nanoparticle therapeutics. Nat. Nanotechnol. 16, 266–276. https://doi.org/10.1038/s41565-021-00858-8.

Russo, E., Selmin, F., Baldassari, S., Gennari, C.G.M., Caviglioli, G., Cilurzo, F., Minghetti, P., Parodi, B., 2016. A focus on mucoadhesive polymers and their application in buccal dosage forms. J. Drug Deliv. Sci. Technol. 32, 113–125. https://doi.org/10.1016/j.jddst.2015.06.016.

Rusznyák, Á., Malanga, M., Fenyvesi, É., Szente, L., Váradi, J., Bácskay, I., Vecsernyés, M., Vasvári, G., Haimhoffer, Á., Fehér, P., Ujhelyi, Z., Nagy, B., Fejes, Z., Fenyvesi, F., 2021. Investigation of the cellular effects of beta-cyclodextrin derivatives on Caco-2 intestinal epithelial cells. Pharmaceutics 13, 1–14. https://doi.org/10.3390/pharmaceutics13020157.

Safwat, S., Ishak, R.A.H., Hathout, R.M., Mortada, N.D., 2017. Nanostructured lipid carriers loaded with simvastatin: effect of PEG/glycerides on characterization, stability, cellular uptake efficiency and in vitro cytotoxicity. Drug Dev. Ind. Pharm. 43, 1112–1125. https://doi.org/10.1080/03639045.2017.1293681.

Srivastava, G.K., Reinoso, R., Singh, A.K., Fernandez-Bueno, I., Hileeto, D., Martino, M., Garcia-Gutierrez, M.T., Pigazo Merino, J.M., Alonso, N.F., Corell, A., Pastor, J.C., 2011. Trypan Blue staining method for quenching the autofluorescence of RPE cells for improving protein expression analysis. Exp. Eye Res. 93, 956–962. https://doi.org/10.1016/j.exer.2011.07.002.

Thielbeer, F., Donaldson, K., Bradley, M., 2011. Zeta potential mediated reaction monitoring on nano and microparticles. Bioconjug. Chem. 22, 144–150. https://doi.org/10.1021/bc1005015.

Torres, A.G., Gait, M.J., 2012. Exploiting cell surface thiols to enhance cellular uptake. Trends Biotechnol. 30, 185–190. https://doi.org/10.1016/j.tibtech.2011.12.002.

Ujhelyi, Z., Fenyvesi, F., Váradi, J., Fehér, P., Kiss, T., Veszelka, S., Deli, M., Vecsernyés, M., Bácskay, I., 2012. Evaluation of cytotoxicity of surfactants used in self-micro emulsifying drug delivery systems and their effects on paracellular transport in Caco-2 cell monolayer. Eur. J. Pharm. Sci. 47, 564–573. https://doi.org/10.1016/j.ejps.2012.07.005.

Van Amersfoort, E.S., Van Strijp, J.A.G., 1994. Evaluation of a flow cytometric fluorescence quenching assay of phagocytosis of sensitized sheep erythrocytes by polymorphonuclear leukocytes. Cytometry 17, 294–301. https://doi.org/10.1002/cyto.990170404.

Vercauteren, D., Vandenbroucke, R.E., Jones, A.T., Rejman, J., Demeester, J., De Smedt, S.C., Sanders, N.N., Braeckmans, K., 2010. The use of inhibitors to study endocytic pathways of gene carriers: Optimization and pitfalls. Mol. Ther. 18, 561–569. https://doi.org/10.1038/mt.2009.281.

Wang, J., Li, L., Du, Y., Sun, J., Han, X., Luo, C., Ai, X., Zhang, Q., Wang, Y., Fu, Q., Yang, Z., He, Z., 2015. Improved oral absorption of doxorubicin by amphiphilic copolymer of lysine-linked ditocopherol polyethylene glycol 2000 succinate: In vitro characterization and in vivo evaluation. Mol. Pharm. 12, 463–473. https://doi.org/10.1021/mp500833m.

Wibel, R., Braun, D.E., Hämmerle, L., Jörgensen, A.M., Knoll, P., Salvenmoser, W., Steinbring, C., Bernkop-Schnürch, A., 2021. In Vitro Investigation of Thiolated Chitosan Derivatives as Mucoadhesive Coating Materials for Solid Lipid Nanoparticles. Biomacromolecules. https://doi.org/10.1021/acs.biomac.1c00776.

Yamabhai, M., Anderson, R.G.W., 2002. Second cysteine-rich region of epidermal growth factor receptor contains targeting information for caveolae/rafts. J. Biol. Chem. 277, 24843–24846. https://doi.org/10.1074/jbc.C200277200.